Polydopamine Nanoparticles as a Potential Non-Pharmaceutical Antioxidant Tool against Mitochondrial Disorders

ACS APPLIED NANO MATERIALS

www.acsanm.org

Article

Polydopamine Nanoparticles as a Potential Non-Pharmaceutical Antioxidant Tool against Mitochondrial Disorders

Matteo Battaglini,* Francesco Schiavone, Alessio Carmignani, Attilio Marino, Valentina Naef, Andrea Petretto, Martina Bartolucci, Fabiana Longo, Francesca Maltecca, Filippo Maria Santorelli, and Gianni Ciofani*

Cite This: *ACS Appl. Nano Mater.* 2025, 8, 16540−16552

Read Online

ACCESS | Metrics & More | Article Recommendations | Supporting Information

ABSTRACT: Mitochondrial disorders are hereditary diseases caused by mutations in nuclear or mitochondrial DNA that impair organelle function. Key features include excessive production of reactive oxygen species (ROS), mitochondrial abnormalities, and metabolic dysfunctions. Systemically, these defects can lead to severe conditions affecting the central nervous system, muscles, heart, and gastrointestinal tract. Organic antioxidants such as idebenone and resveratrol have been explored as potential treatments; in the framework of nanotechnological antioxidants, polydopamine nanoparticles (PDNPs), derived from the oxidative self-polymerization of dopamine, are highly biocompatible, biodegradable, easy to functionalize, and possess potent ROS-scavenging and photothermal properties. In this study, we investigated PDNPs as a nonpharmaceutical therapy for mitochondrial encephalomyopathy with lactic acidosis and stroke-like episodes (MELAS) and progressive external ophthalmoplegia (PEO). PDNPs were evaluated in fibroblasts from healthy donors and patients with MELAS and PEO. Molecular characterization was performed via proteomic analysis, followed by assessment of PDNP biocompatibility, internalization, intracellular localization, and antioxidant effects. Their protective activity was also confirmed in vivo, exploiting zebrafish embryos. Our findings demonstrate that PDNPs effectively protect cells from ROS-induced damage, oxidative stress, apoptosis, and mitochondrial dysfunction. Additionally, PDNPs were able to preserve zebrafish embryos against pro-oxidative stimuli. Overall, this work highlights the potential of polydopamine nanostructures as promising therapeutic tools for mitigating the molecular hallmarks of mitochondrial disorders and supporting future clinical applications.

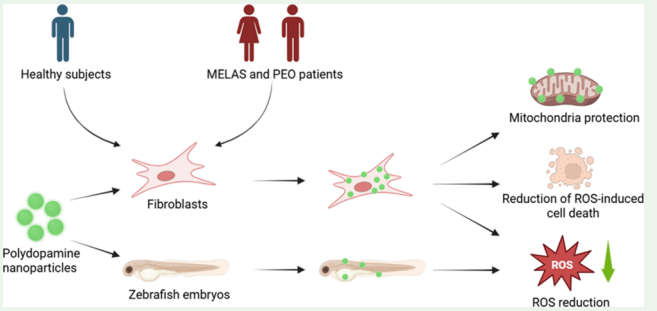

KEYWORDS: *poydopamine nanoparticles, mitochondrial diseases, oxidative stress, mitochondrial encephalomyopathy with lactic acidosis and stroke-like episodes, progressive external ophthalmoplegia*

1. INTRODUCTION

Mitochondrial diseases are a subset of genetic disorders caused by mutations in genes in the nuclear DNA (nDNA) and/or in the mitochondrial DNA (mtDNA) encoding proteins involved in mitochondrial organization and functions.[1] Mitochondrial diseases represent the most common family of inherited metabolic disorders, and are the most common cause of congenital neurological impairments.[1] Some of the molecular hallmarks include DNA damage, oxidative damage, defective oxidative phosphorylation, nucleotide pool imbalances, and altered mitochondrial biogenesis, morphology, and functions.[1−3]

The use of antioxidant moieties as a countermeasure for the oxidative stress associated with mitochondrial disorders has been proposed as a potential therapeutic strategy for these diseases. Some of the exploited antioxidants include resveratrol,[4] idebenone[5] and N-acetylcysteine (NAC).[6] Despite their potential, the effectiveness of conventional antioxidant compounds is limited by several factors, including low bioavailability and low ability to cross the blood−brain barrier (BBB) and reach the central nervous system (CNS).[7] Antioxidant nanomaterials have been proposed as an alternative to conventional antioxidant drugs.[7−10] In this view, one of the most promising classes of nanomaterials is represented by polydopamine nanoparticles (PDNPs). As the name implies, PDNPs are obtained from the self-polymerization of dopamine. PDNPs are characterized by several interesting properties, which include a high level of biocompatibility and biodegradability, high

Received: July 4, 2025
Revised: August 1, 2025
Accepted: August 1, 2025
Published: August 7, 2025

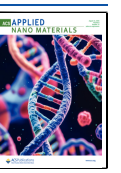

antioxidant capacities, the ability to be easily tuned in terms of size, porosity, and surface functionalization, and the possibility to be exploited as near-infrared (NIR) photothermal conversion agents.[11] The antioxidant properties of PDNPs have been exploited as a potential treatment for several human disorders, including Parkinson's disease,[12] Alzheimer's disease,[13] ischemia,[14] liver steatosis,[15] and skin wounds.[16] In a previous work from our group we tested the potential of PDNPs as a treatment for autosomal recessive spastic ataxia of Charlevoix-Saguenay (ARSACS), demonstrating the ability of polydopamine nanostructures to counteract some of the molecular hallmarks of the disease.[17]

In this work, we focused our analysis on the exploitation of PDNPs as an antioxidant treatment against two mitochondrial disorders, namely mitochondrial encephalomyopathy with lactic acidosis and stroke-like episodes (MELAS) and progressive external ophthalmoplegia (PEO). MELAS is a multiorgan disease with several symptoms which include diabetes, hearing impairments, myopathy, stroke-like episodes, dementia, and epilepsy. MELAS is caused by mutations in the mtDNA (the most common mutation is represented by the m.3243A > G mutation in the *MT-TL1* gene encoding the mitochondrial tRNALeu (UUR), which affects the normal mitochondrial protein synthesis and translation, leading to impairments in the mitochondrial energy production.[18] PEO disease is characterized by ptosis and impaired eye movements[19]; from a molecular point of view, PEO has been associated with large depletion of mtDNA, which leads to impairments in mitochondrial ATP production.[20] Both diseases are also associated with a high production of reactive oxygen species (ROS), which have been identified as a key factor in the pathological mechanism of the two disorders.[21,22] Several antioxidant compounds have been proposed and tested to ameliorate the mitochondrial impairments and oxidative stress associated with both conditions, including L-carnitine, coenzyme Q10, cysteine, arginine, riboflavin, thiamine, vitamin C, E, idebenone, and resveratrol.[23−27] As already stated, despite their potential, traditional antioxidants are limited by poor bioavailability and a relatively low BBB permeability:[7] in this regard, the exploitation of PDNPs could represent an innovative approach.[11]

PDNPs have been reported to efficiently cross cell membranes and be internalized by cells through multiple endocytic pathways. Notably, the uptake mechanism is strongly influenced by particle size and morphology. Acter et al. demonstrated that smaller mesoporous PDNPs (∼180 nm) are preferentially internalized via macropinocytosis, whereas larger particles (∼520 nm) primarily enter cells through caveolae-mediated endocytosis.[28] In addition, Ding et al. showed that PDNPs can also be internalized through Arf6-dependent endocytosis and Rab34-mediated macropinocytosis.[29] These observations highlight that the physicochemical characteristics of PDNPs are key determinants of their cellular uptake and intracellular distribution, supporting their use as versatile nanocarriers for therapeutic applications.

We exploited fibroblasts derived from healthy subjects and from MELAS and PEO patients as a model of mitochondrial diseases. The three cell lines were first fully characterized in terms of protein expression through proteomic analysis; then, PDNPs were tested in terms of biocompatibility, internalization, intracellular localization, and antioxidant protective effects. In particular, the ability of PDNPs to counteract ROS production, prevent oxidative stress-induced cellular death, and prevent mitochondrial aberrations was tested. Eventually, the antioxidant effects of PDNPs were confirmed on an in vivo model based on zebrafish embryos. Fibroblasts were chosen for several reasons; first, primary fibroblasts are widely used patient-derived cell models to study mitochondrial disorders because they retain the patients' mitochondrial DNA mutations and accurately recapitulate key disease-related bioenergetic defects.[30,31] Additionally, skin fibroblasts can be obtained through minimally invasive biopsies, thereby avoiding the need for neural tissue sampling.[32]They are also easy to culture and well-suited for reproducible high-content assays, proteomic analyses, and oxidative stress testing.[33] Finally, numerous studies have validated fibroblasts as reliable models for investigating mitochondrial pathophysiology and for screening potential therapeutic approaches.[34]

2. MATERIALS AND METHODS

2.1. PDNP Synthesis and Characterization. PDNPs were fabricated exploiting the Stöber reaction method with some modifications, as previously described.[35] Briefly, a mixture of concentrated ammonium hydrochloride (4 mL, NH_4OH, Sigma-Aldrich), ethanol (40 mL), and ultrapure water (90 mL) was stirred at 400 rpm for 30 min at room temperature. Thereafter, 0.5 g of dopamine hydrochloride (Sigma-Aldrich) dissolved in 10 mL of Milli-Q water was added to the mixture and left under agitation for 24 h. The obtained dispersion was then diluted 1:4 with ethanol, and PDNPs were collected through four centrifugation steps and rinsing in ultrapure water (the first centrifugation step was carried out at 10,860*g* for 30 min at 4 °C while the subsequent three steps were performed at 21,300*g* for 1 h and 30 min at 4 °C).

PDNPs were quantified after freeze-drying and characterized through scanning electron microscopy (SEM) and transmission electron microscopy (TEM). For SEM analysis, a dual-beam SEM system was exploited (HeliosNanoLab 600i). Samples were dropped cast on a silicon substrate and let dry under a chemical hood, and then gold sputtered with a Quorum SC7620 mini-Gold Sputter Coater (15 mA for 30 s). The images obtained were analyzed using Gwydion software. For TEM imaging, PDNP dispersions were sonicated (20 min) and drop-cast on a Cu TEM grid of 200 hexagonal mesh. TEM analyses were performed exploiting a JEOL JEM 1011 electron microscope and recorded with a 2 MP charge-coupled device camera (Orius Gatan). Before imaging, PDNPs were stained with 1% uranyl acetate in Milli-Q water for 1 min.

PDNPs were then characterized through dynamic light scattering (DLS) analysis for the assessment of hydrodynamic diameter, average surface zeta potential (ζ-potential), and polydispersity index (PDI), using a Malvern Zetasizer Nano ZS90. Measurements were performed at 25 and 37 °C using a 100 μg/mL concentration of PDNPs. Disposable polystyrene cuvettes (Malvern Zetasizer Nano series) were used for hydrodynamic diameter and PDI measurements, while folded capillary cells (Malvern Zetasizer Nano series) for ζ-potential measurements.

2.2. Primary Fibroblast Cell Culture. Primary skin fibroblasts were obtained from biopsies derived from the skin of MELAS (m.3243A > G mutation with 14% heteroplasmy in muscle) and PEO (muscular mtDNA heteroplasmic microdeletion) patients, while normal human dermal fibroblasts (NHDF) were purchased from the American Type Culture Collection (C-12302, Sigma-Aldrich). This investigation conformed to principles outlined in the Declaration of Helsinki, and patients signed informed consent before skin biopsy procedure. All the cells were cultured using high glucose Dulbecco's modified Eagles's medium (DMEM, EuroClone) supplemented with 20% of heat-inactivated fetal bovine serum (FBS, Sigma-Aldrich), 1 mM sodium pyruvate (EuroClone), 100 IU/mL of penicillin (EuroClone), and 100 μg/mL of streptomycin (EuroClone). Cells were cultured at 37 °C in a humidified atmosphere with 5% CO_2.

2.3. Proteomic Analysis. NHDFs, MELAS-derived and PEO-derived cells were seeded in 25 cm^2 tissue culture flasks (Corning).

https://doi.org/10.1021/acsanm.5c03169
ACS Appl. Nano Mater. 2025, 8, 16540−16552

Upon reaching approximately full confluency, cells were detached through trypsinization, washed in Dulbecco's phosphate-buffered saline (DPBS, EuroClone) and frozen at −80 °C. Pellets were then lysed, reduced, and alkylated in 50 μL LYSE buffer (Preomics) at 95 °C for 10 min and sonicated with an Ultrasonic Processor UP200 St (Hielscher), 3 cycles of 30 s. To remove the nanoparticles, samples were centrifuged at 20,000*g* at 4 °C for 20 min. Proteins were isolated and digested by the PAC method automated on a KingFisher Apex robot (Thermo Fisher Scientific) in a 96-well format as previously described.[36] Briefly, the tip plate was stored in plate #1. Lysate samples were stored in plate #2, in a final concentration of 70% acetonitrile and with magnetic beads in a protein/bead ratio of 1:4 (1:1 SpeedBead Magnetic Carboxylate, 45152105050250 and 65152105050250). Washing solutions were in plates #3−5 (acetonitrile), plate #6 (70% ethanol), and plate #7 (isopropanol). Plate #8 contained 100 μL digestion solution of 25 mM Tris HCl pH 8, LysC (Wako) in an enzyme:protein ratio of 1:100 (w/w), and trypsin (Promega) in an enzyme:protein ratio of 1:50. The protein aggregation was carried out in two steps of 1 min mixing at medium mixing speed, followed by a 10 min pause each. The sequential washes were performed in 2.5 min and slow speed, without releasing the beads from the magnet. The digestion was set to 4 h at 37 °C with slow speed.

Resulting peptides were analyzed on the Evosep One system using an EASY spray column (150 μm × 15 cm, 2 μm particle size, Thermo Scientific) and the preprogrammed gradient of 30 samples per day, with a flow rate of 0.5 μL/min. The column temperature was maintained at 40 °C and interfaced online with the Orbitrap Exploris 480 Mass Spectroscopy (MS, Thermo Scientific) with high-field asymmetric waveform ion mobility spectrometry (FAIMS), Pro Duo Interface (Thermo Scientific). MS analysis was performed in DIA mode. FAIMS CV was set to −45 at standard resolution. Full MS resolution was set to 120,000 in a range between 375 and 1500 m/z and with a normalized automatic gain control (AGC) target of 300% with a maximum IT set to Auto. The normalized AGC target value for fragment spectra was set at 1000%. 40 windows of 15 Da were used with an overlap of 1 Da. The resolution was set to 30,000 and IT to Auto. The normalized collision energy was set at 30%. All data were acquired in profile mode using positive polarity.

2.4. PDNP Biocompatibility. The PDNP effects on primary fibroblasts were evaluated using the Quanti-iT PicoGreen dsDNA assay Kit (Invitrogen) and the Live/Dead assay (Thermo Fisher). For PicoGreen analysis, NHDFs and patient-derived fibroblasts (10,000 cells/cm^2) were seeded in a 96-well plate (Sarstedt) and incubated with increasing concentrations of PDNPs (0.00, 31.25, 62.50, 125.00, and 250.00 μg/mL) for 72 h. After PDNP treatment, cells were washed with Dulbecco's phosphate-buffered saline (DPBS EuroClone), suspended in 100 μL of Milli-Q, and exposed to three freeze−thaw cycles from −80 to 37 °C. PicoGreen was carried out in Corning Costar 96-well black polystyrene plates as per the manufacturer's instructions. The samples were then assessed with a Victor X3Multilabel Plate Reader, and the fluorescence intensity (λ_{ex} 485, λ_{em} 535 nm; PerkinElmer) was put in relation with cell number, and thus with proliferation.

For Live/Dead assay, NHDFs and patient-derived fibroblasts were seeded (10,000 cells/cm^2) in a 24-well plate (Corning) and incubated for 72 h with PDNPs at different concentrations (0.00, 31.25, 62.50, 125.00, and 250.00 μg/mL). Thereafter, cells were washed with DPBS and incubated for 30 min at 37 °C with phenol red-free medium containing 5 μg/mL of Hoechst 33342 for nucleus staining (Invitrogen), 4 μM of ethidium homodimer-1 for the staining of dead cells, and 2 μM of calcein-AM for the staining of viable cells (all reagents from Thermo Fisher). After the staining, cells were washed with DPS and imaged using a fluorescence microscope (Eclipse Ti, Nikon) with a 10× objective. Acquired images were analyzed using ImageJ software.

2.5. PDNP Internalization and Intracellular Localization. The internalization and intracellular localization of PDNPs in NHDFs and patient-derived fibroblasts were evaluated through flow cytometry and confocal microscopy. PDNPs were labeled with DiO-dye (Vybrant Multicolor Cell-Labeling Kit, Thermo Fisher). Briefly, 20 μM of DiO-dye were added to 1 mL of Milli-Q water containing 7 mg/mL of PDNPs and left under stirring at room temperature for 3 h. The obtained DiO-PDNPs were washed with ultrapure water three times at 213,000*g* for 90 min at 4 °C.

For flow cytometry analysis, cells were seeded in a 24-well plate (Corning) and incubated with phenol red-free medium containing 100 μg/mL of DiO-PDNPs. Cells were then detached and analyzed through flow cytometry (CytoFLEX platform, Beckman Coulter, λ_{ex} 488, λ_{em} 525 nm).

The intracellular localization and uptake of DiO-PDNPs were evaluated with confocal microscopy (C 2s system, Nikon, equipped with a 60× oil immersion objective). Cells were seeded in a 96-well μ-Plate black (Ibidi-cells in focus) and incubated with phenol red-free medium containing 100 μg/mL of DiO-PDNPs; thereafter, cells were washed in DPBS and treated for 30 min at 37 °C with a solution composed of phenol red-free medium containing either 5 μM of Lysotracker-Red (Thermo Fisher) and 5 μg/mL Hoescht 33342 (Invitrogen) for lysosomes imaging or with a solution containing tetramethylrhodamine methyl ester (TMRM, Life Technologies) and 5 μg/mL Hoescht 33342 (Invitrogen) for mitochondrial imaging. Images were acquired after 4, 24, and 72 h of treatment with DiO-PDNPs.

2.6. PDNP Antioxidant and Protective Properties: In Vitro Analysis. Cells were seeded (10,000 cells/cm^2) in 6-well plates (Corning) and incubated with and without 100 μg/mL of PDNPs for 72 h. After the incubation, cells were treated in phenol red-free medium using CellROX Green reagent 2.5 μM (Invitrogen) for 30 min at 37 °C. Thereafter, cells were detached through trypsinization and separated into individual flow cytometry tubes. Half the samples were exposed to 2.5 mM of tertbutyl hydroperoxide solution (TBH, Sigma-Aldrich) for 30 min at room temperature. The relative fluorescence intensities of all the experimental conditions (CTRL, TBH, PDNPs, and PDNPs + TBH) were measured through flow cytometry (λ_{ex} 488, λ_{em} 525 nm).

To evaluate the capacity of PDNPs to prevent ROS-induced apoptosis, cells were once again seeded (10,000 cells/cm^2) in 6-well plates (Corning) and incubated with and without 100 μg/mL of PDNPs for 72 h. Thereafter, cells were incubated with different concentrations of TBH (0, 100, and 250 μM) for 24 h, and then detached through trypsinization and stained with annexin V-FITC/propidium iodide (PI) as per the manufacturer's instructions (FITC Annexin/Dead Cell Apoptosis kit, Thermo Fisher). After the staining, cells were resuspended in 500 μL of DPBS and analyzed through flow cytometry (for annexin V-FITC λ_{ex} 488, λ_{em} 525 nm; for PI λ_{ex} 488, λ_{em} 610 nm).

2.7. PDNP Protective Effects against ROS-Induced Mitochondrial Aberrations. PDNP ability to prevent ROS-induced damage on mitochondrial morphology was tested. Cells were seeded (10,000 cells/cm^2) in Willco dishes (GWST-3512) and let grow for 24 h and then incubated with 100 μg/mL of PDNPs. After 72 h, cells were treated for 40 min in phenol red-free medium with or without 2.5 mM of TBH. Cells were then labeled with 1 μM tetramethylrhodamine methyl ester (TMRM, Life Technologies) for 1 h at 37 °C and rinsed twice with DPBS (Sigma). Finally, cells were incubated in phenol red-free media (supplemented with HEPES 25 mM, Thermo Fisher), and imaged through confocal microscopy (C 2s system, Nikon). Images were analyzed through the Fiji software, exploiting the mitochondria analyzer plugin. Mitochondrial morphology was described in terms of mitochondrial area (cm^2), mean form factor, ratio between mitochondrial branches and mitochondria number, and ratio between branch junctions and mitochondria number.

2.8. PDNP Antioxidant Properties: In Vivo Analysis. Casper-adult zebrafishes (*Danio rerio*) were kept in a laboratory fish tank at 28 °C with a cycle of 14:10 h of light: dark, in a closed flow-through system with charcoal-filtered tap water.[37] Zebrafish eggs and embryos were collected and raised at 28.5 °C in E3 medium using established procedures and staged in "hours post fertilization" (hpf) or "days post fertilization" (dpf).[37] Zebrafish handling and experimental procedures were performed under the supervision of the Animal Care and Use Committee of the IRCCS Stella Maris Foundation (Pisa, Italy), in compliance with European Directive No. 63 on protecting animals used for research, dated September 22, 2010.[38]

https://doi.org/10.1021/acsanm.5c03169
ACS Appl. Nano Mater. 2025, 8, 16540−16552

PDNP dispersions were prepared at concentrations of 12.5 and 25.0 μg/mL in E3 medium. All treatments have been performed in triplicate with 10 embryos per replicate, and lasted from 24 to 120 hpf in a dark environment without media replacement. To assess the antioxidant activity of the nanoparticles, we first measured ROS levels under basal conditions[39] and then after adding the pro-oxidant TBH at 2 mM for 2 h; cytoplasmatic ROS levels were evaluated using the fluorescent probe H2DCFDA (1 mM), as previously described.[40] A lateral image of each larva was obtained with a fluorescence microscope (Leica, MDG41), and the fluorescence intensity in a region of interest (ROI) was quantified using the ImageJ 64 software. The results were then normalized to the background fluorescence.

2.9. Statistical Analysis. Statistical analyses were carried out using R software. Data normality was evaluated through the Shapiro-Test. Normally distributed data were analyzed using the ANOVA test followed by the LSD post hoc test with Bonferroni's correction for multiple comparisons. The data were then expressed as mean ± standard deviation. All experiments were conducted in triplicate ($n = 3$) unless otherwise specified.

All data-independent acquisition (DIA) raw files derived from the proteomic analysis were processed with Spectronaut version 18[41] using a library-free approach (directDIA) under default settings. Enzymes/Cleavage Rules were set to Trypsin/P, LysC. The library was generated against the Uniprot Human database (release UP000005640_9606 June 2024). Carbamidomethylation was selected as a fixed modification, while methionine oxidation and N-terminal acetylation were selected as variable modifications. False Discovery rates (FDRs) of peptide-spectrum matches (PSMs) and peptide/protein groups were set to 0.01. For quantification Precursor Filtering was set to Identified (Qvalue), Imputation Strategy was set to None and MS2 was chosen as quantity MS-level. The Protein Quant Pivot Report generated by Spectronaut was statistically evaluated using Perseus software[42] version 1.6.15.0. GO enrichment was obtained with the Web server HumanBase[43] with "skin fibroblast" as background.

3. RESULTS

3.1. PDNP Characterization. As shown in Figure 1a,b, SEM and TEM images highlight nanostructures with a spherical shape, uniform in terms of size and morphology and with an average diameter of 94.59 ± 4.14 nm. DLS results, reported in Figure 1c, show monodisperse size distributions (PDI values of 0.117 ± 0.021 and 0.201 ± 0.038 at 25 and 37 °C, respectively) with a hydrodynamic diameter of 112.8 ± 0.3 nm at 25 °C and 115.4 ± 2.3 nm at 37 °C. ζ-potential values of PDNPs, as shown in Figure 1d, were −42.3 ± 0.9 mV at 25 °C and −37.6 ± 0.2 mV at 37 °C.

3.2. Proteomic Analysis. Proteomic analysis was carried out to characterize the molecular differences between healthy fibroblasts and patient-derived cells. The comparison between healthy fibroblasts and MELAS-derived fibroblasts demonstrated the presence of 782 downregulated and 939 upregulated proteins in MELAS cells (Figure S1). GO analysis for biological functions shown in Figures S2 and S3 highlights he presence of altered terms, and in particular metabolic pathways involved in the cell cycle regulation, mRNA synthesis and maturation, chromatin organization, mitochondrial morphology and functions, protein synthesis, maturation, and intracellular localization. The comparison of PEO-derived fibroblasts with healthy fibroblasts is shown in Figure S4 and demonstrates the presence of 1035 downregulated and 976 upregulated proteins in PEO cells. Once again, GO analysis for biological functions shown in Figures S5 and S6 demonstrates the presence of altered terms involved in mitochondrial and respiratory chain organization and functions, cell cycle regulation, production of inflammatory factors, protein synthesis, maturation, and intracellular localization.

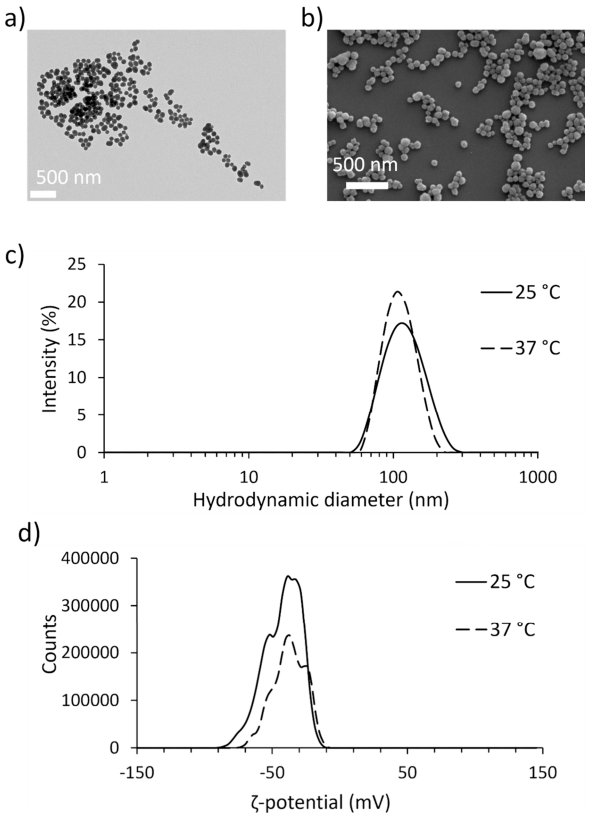

Figure 1. Representative (a) SEM and (b) TEM images of PDNPs. (c) Average hydrodynamic diameter and (d) ζ-potential of PDNP dispersions in water at the two different tested temperatures.

3.3. PDNP Biocompatibility. The effects of PDNPs on cell viability and proliferation were assessed on fibroblasts derived from healthy subjects, MELAS, and PEO patients. As shown in Figures S7−S9, a high level of live cells (calcein-positive cells, in green) was observed in all the experimental conditions and no statistically significant difference ($p > 0.05$; Figure S10) was observed in terms of dead cells (propidium iodide-positive cells, in red). These results were confirmed by the Picogreen assay (Figure S11), where no statistically significant difference was observed for any of the tested concentrations and on all the cell types in terms of dsDNA cellular content (and thus in terms of cell proliferation).

Based on these results, the experiments reported in the following sections were carried out exploiting a working PDNP concentration of 100 μg/mL, based also on earlier reports on the antioxidant capacities of these nanostructures.[35]

3.4. PDNP Internalization and Intracellular Localization. To evaluate cellular internalization, healthy and patient-derived cells were incubated with DiO-labeled PDNPs at 100 μg/mL for 4, 24, and 72 h, and their relative fluorescence level was assessed through flow cytometry. Figure 2 shows the results of the analysis, where the percentage of cells positive or negative for PDNP signal is reported (FITC+ and FITC-, respectively). We observed in all the three cell typologies a high degree of internalization after 24 and 72 h of incubation, in particular the analysis showed approximately 75% of FITC+ cells after 24 h and 95% after 72 h in healthy fibroblasts, 15% of FITC+ cells after 24 h and 35% after 72 h in MELAS-derived fibroblasts, and approximately 20% of FITC+ cells after 24 h and 60% after 72 h in PEO-derived fibroblasts (representative histograms reported in Figure S12).

https://doi.org/10.1021/acsanm.5c03169
ACS Appl. Nano Mater. 2025, 8, 16540−16552

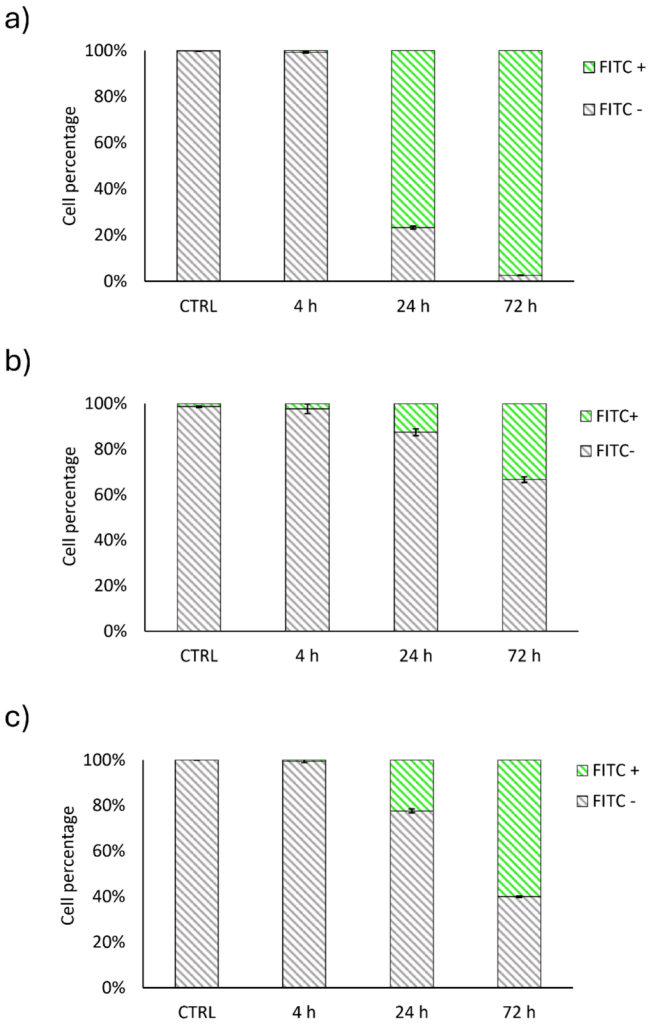

Figure 2. Flow cytometry analysis of (a) healthy fibroblasts, (b) fibroblasts derived from MELAS patients, and (c) fibroblasts derived from PEO patients incubated with DiO-PDNPs at different time points (4, 24, and 72 h), with respect to control cultures.

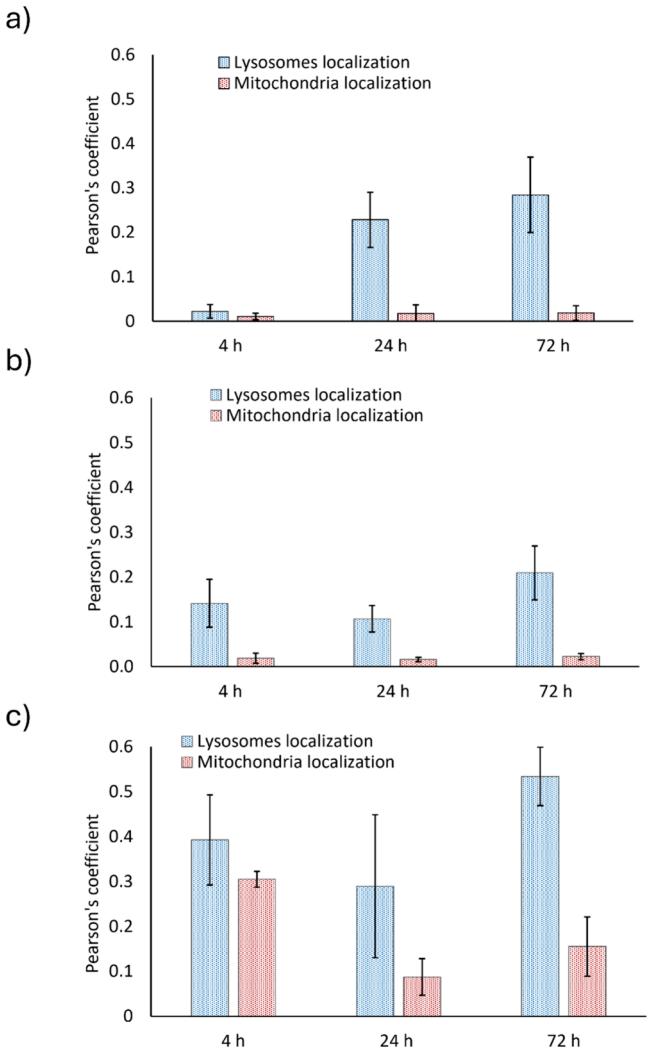

Figure 3. Analysis of the intracellular localization of PDNPs in (a) healthy fibroblasts, (b) fibroblasts derived from MELAS patients, and (c) fibroblasts derived from PEO patients.

Intracellular localization analysis is shown in Figure 3. As for the previous experiment, cells were treated with 100 μg/mL for 4, 24, and 72 h with DiO-labeled PDNPs and subsequently imaged through confocal microscopy. The Pearson's correlation coefficient analysis assessing the colocalization between PDNPs and lysosomes (blue bars in the graphs) and mitochondria (red bars in the graphs) is reported for fibroblasts derived from healthy subjects (Figure 3a) and for fibroblasts derived from MELAS (Figure 3b) and PEO (Figure 3c) patients. In all the three cell line we observed a relatively high localization of PDNPs in lysosomes (Pearsons's correlation coefficient after 72 h equal to 0.28 in healthy fibroblasts, 0.20 in MELAS-derived fibroblasts and 0.53 in PEO-derived fibroblasts), and almost no localization in mitochondria (0.018 in healthy fibroblasts, 0.022 in MELAS-derived fibroblasts, and 0.15 in PEO-derived fibroblasts). Representative confocal images of these analyses are shown in Figures S13−S15.

3.5. PDNP Antioxidant Properties: In Vitro Analysis. The ability of PDNPs to counteract ROS accumulation was assessed through flow cytometry. The results are shown in Figure 4a for healthy fibroblasts, Figure 4b for MELAS-derived cells, and Figure 4c for PEO-derived cells, while representative histograms are shown in Figure S16. In all the cell typologies, we observed a statistically significant increase of the overall ROS level ($p < 0.001$), which was partially counteracted by the treatment with PDNPs ($p < 0.001$). Moreover, as shown in Table S1, the statistical analysis demonstrated a significant difference ($p < 0.001$) between the amount of ROS accumulated after TBH treatment in healthy cells with respect to MELAS and PEO fibroblasts.

The ability of PDNPs to prevent ROS-induced cellular death was moreover assessed as shown in Figure 5a for healthy fibroblasts, Figure 5b for MELAS-derived fibroblasts, and Figure 5c for PEO-derived fibroblasts (representative scatter plots in Figure S17). We observed a statistically significant reduction of the overall number of viable cells following the treatment with 250 μM TBH in all cell typologies ($p < 0.001$). This reduction was partially prevented in the case of the treatment with PDNPs, which were able to avoid the induction of apoptosis and/or necrosis caused by the treatment with either 100 or 250 μM of TBH (a statistically significant difference was observed in all the comparison between cells treated with only TBH and with the combination of PDNPs + TBH, with a $p < 0.001$).

3.6. PDNP Protective Effects against ROS-Induced Mitochondrial Aberrations. The ability of PDNPs to prevent ROS-induced mitochondrial aberrations was assessed through

https://doi.org/10.1021/acsanm.5c03169
ACS Appl. Nano Mater. 2025, 8, 16540−16552

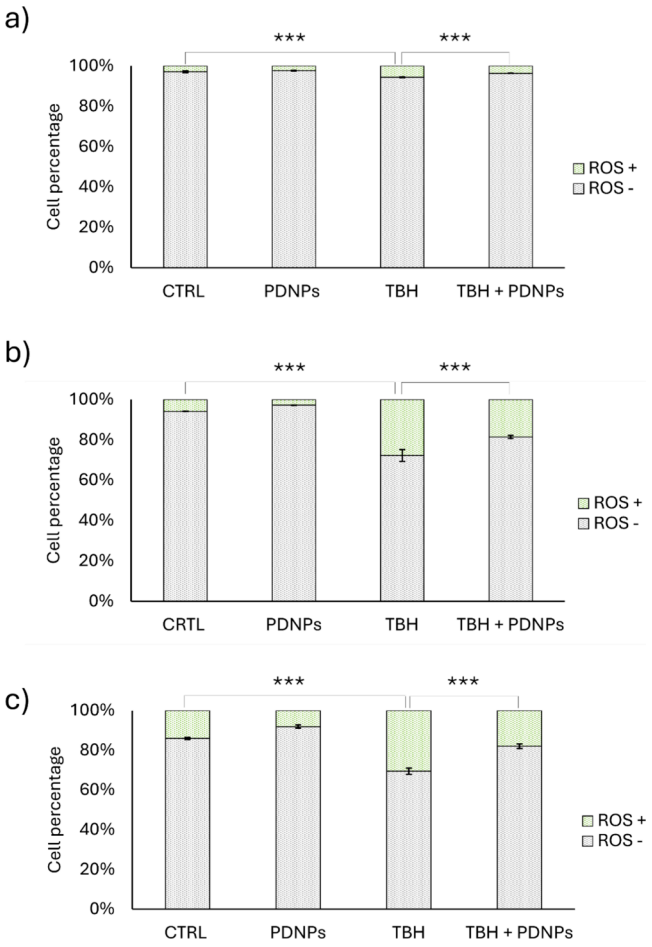

Figure 4. Analysis of the antioxidant properties of PDNPs in (a) healthy fibroblasts, (b) fibroblasts derived from MELAS patients, and (c) fibroblasts derived from PEO patients. The graphs show the % of ROS positive (ROS+) and ROS negative (ROS−) cells assessed by flow cytometry following CellRox staining (***$p < 0.001$).

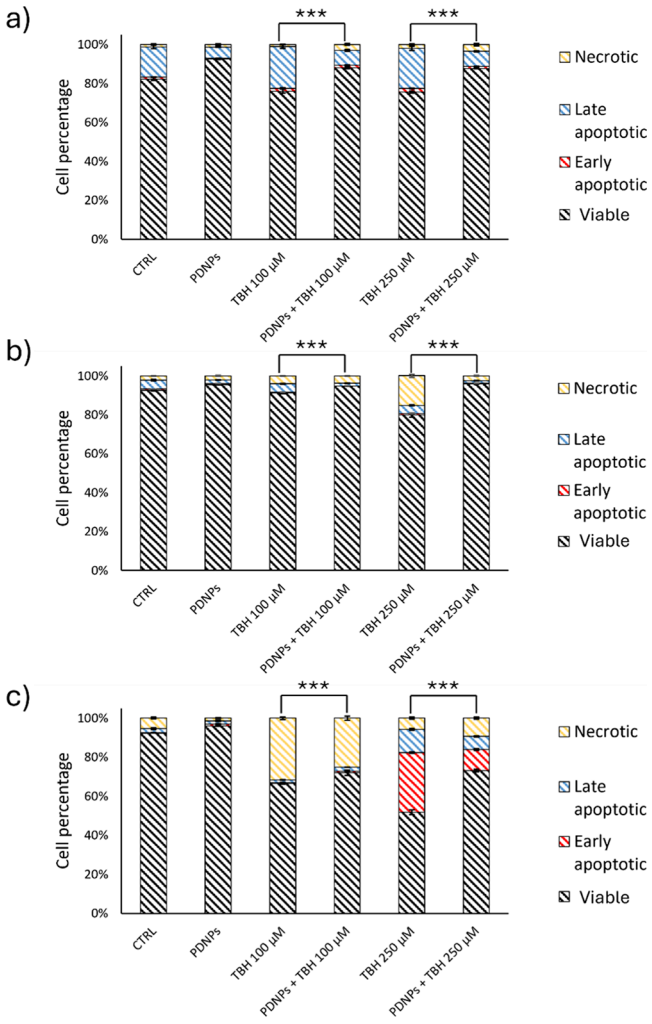

Figure 5. Evaluation of apoptosis/necrosis levels through flow cytometry upon annexin-V-FITC/PI staining on (a) healthy fibroblasts, (b) fibroblasts derived from MELAS patients, and (c) fibroblasts derived from PEO patients upon different experimental treatments (***$p < 0.001$).

confocal microscopy, analyzing the surface area covered by mitochondria, the shape factor of mitochondria, the number of mitochondrial branches/mitochondria, and the number of mitochondrial branches junctions/mitochondria. Figure 6 shows the results of the mitochondrial morphology analysis carried out on healthy fibroblasts. We observed that the treatment with TBH induced a significant reduction in the four analyzed parameters, and this reduction was partially prevented by the treatment with PDNPs ($p < 0.05$). In the case of MELAS-derived cells, instead (Figure 7), the treatment with PDNPs was unable to significantly prevent the decrement of the mitochondrial surface area, but indeed hindered the reduction of the other three analyzed parameters ($p < 0.05$ for mean form factor and ratio between branch junctions and mitochondria number; $p < 0.001$ for the ratio between mitochondrial branches and mitochondria number). Concerning PEO-derived cells (Figure 8) a trend similar to that one observed for healthy fibroblasts was found: TBH induced a significant reduction of the four analyzed parameters, and PDNPs partially, but significantly, rescued this decrement ($p < 0.01$ for mitochondrial area, mean form factor and ratio between mitochondrial branches and mitochondria number; $p < 0.05$ for the ratio between mitochondrial branches and mitochondria number).

3.7. PDNP Antioxidant Properties: In Vivo Analysis. The ability of PDNPs to reduce ROS levels and prevent oxidative stress was also assessed in zebrafish embryos. As shown in Figure 9, PDNPs at the highest tested concentration (25.0 μg/mL) were able to reduce the level of basal ROS present in the animals in a statistically significant way ($p < 0.01$). Moreover, PDNPs were also able to prevent and reduce ROS accumulation after TBH treatment at both tested concentrations (12.5 and 25.0 μg/mL; $p < 0.001$).

4. DISCUSSIONS

In this work, we tested for the first time the possibility of exploiting PDNPs as a nonpharmaceutical countermeasure to the oxidative stress associated with MELAS and PEO syndromes. We previously reported how the antioxidant activities of PDNPs of 200 nm in size could be a potential countermeasure for neurological disorders such as ARSACS disease.[17] PDNPs at 100 nm were chosen in this work due to their higher antioxidant potential compared to larger nanostructures, as previously reported.[44]

Smaller PDNPs (~100 nm) exhibit a higher specific surface area-to-volume ratio, which increases the density of accessible catechol and quinone groups on the surface, thereby enhancing their radical scavenging capacity.[44] Nanoparticles below 150 nm

https://doi.org/10.1021/acsanm.5c03169
ACS Appl. Nano Mater. 2025, 8, 16540−16552

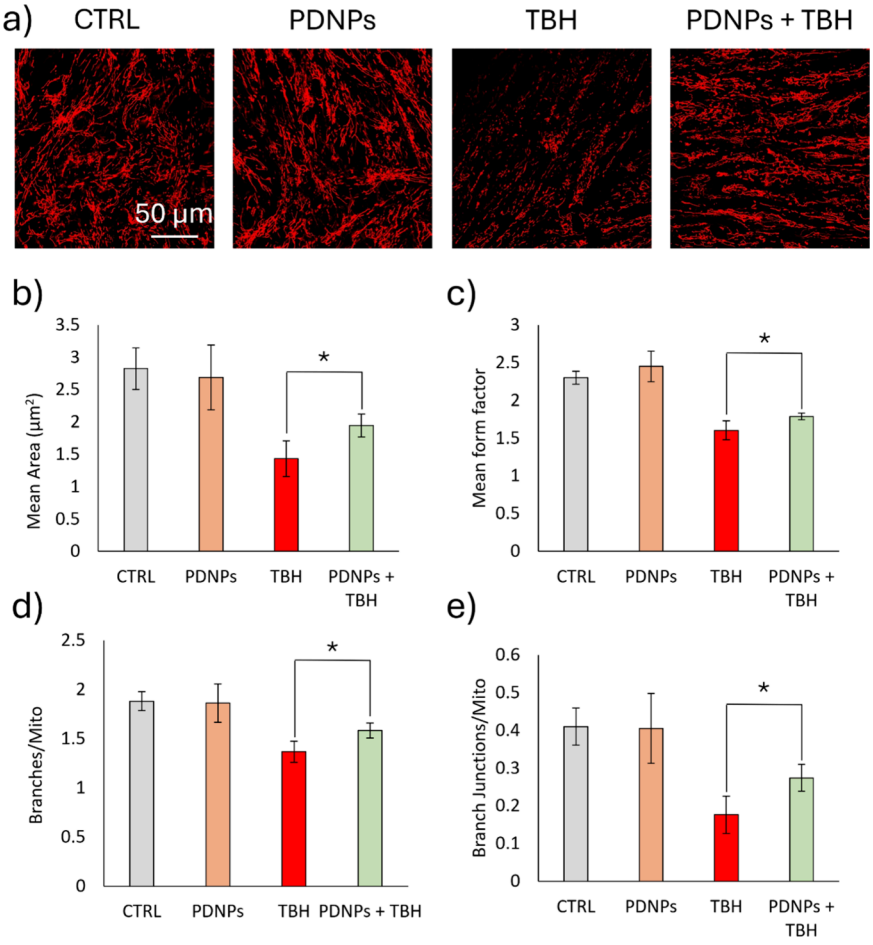

Figure 6. Analysis of mitochondrial morphology in healthy fibroblasts upon different experimental treatments: (a) representative confocal images and quantitative analysis of the (b) mitochondrial area, (c) mean form factor, (d) ratio between mitochondrial branches and mitochondria number, (e) ratio between branch junctions and mitochondria number (* $p < 0.05$).

are more efficiently internalized by cells via endocytosis compared to larger particles[45]; thus, using 100 nm PDNPs could favor higher cellular uptake and more effective intracellular ROS scavenging. 100 nm particles also exhibit greater colloidal stability, lower sedimentation rates, and a lower tendency to aggregate compared to larger particles, which could help maintain consistent bioavailability.[44] From a material design perspective, several structural characteristics other than size of PDNPs play a crucial role in determining their biological interactions and therapeutic performance. Surface roughness and nanoscale texturing, inherent to the self-polymerization process, can enhance adhesion to biological membranes and facilitate protein corona formation, which in turn modulates biodistribution and cellular recognition.[46] Furthermore, the mesoporous architecture of PDNPs increases the accessible surface area: it provides a greater number of active sites for radical scavenging and metal ion chemistry, contributing to their multifunctional antioxidant capacity.[11,47] These interrelated parameters (size, morphology, porosity, and surface chemistry) collectively define the physicochemical profile of PDNPs and can be precisely tuned during synthesis to optimize performance in specific biomedical applications.

Before assessing the protective effects of PDNPs, an in-depth analysis of the proteomic profile of the three cell lines used in this work was carried out. Data showed how MELAS-derived cells present altered molecular pathways in line with what observed from clinical studies conducted on MELAS patients.[18,48,49] The proteomic analysis carried out on PEO cells showed that similar molecular pathways were also altered coherently with literature data, indicating that despite the different genetic defects involved in the pathogenesis of MELAS and PEO diseases, both disorders lead to a similar altered protein expression signature.[50]

Viability analysis proved the absence of toxicity of PDNPs over the three tested cellular types, and no effect of the nanostructures on the cell proliferation, confirming the biocompatibility expected from polydopamine-based nanomaterials.[11] The internalization analysis showed how patient-derived cells were able to uptake nanostructures at a lower extent with respect to healthy fibroblasts, a result ascribable to the metabolic impairments present in MELAS and PEO patients-derived cells, that could affect the physiological uptake and transport system: in support of this hypothesis, for example, it is well-known that MELAS patients' cells present limited uptake of key nutrients such as glutamate and glucose.[51,52] Similar molecular impairments have been observed in the neurons of PEO patients, which have been associated with lower levels of dopamine intake.[43] The different uptake levels of nanostructures from the various cell types could potentially explain the various degree of efficiency of the PDNPs-based antioxidant treatment.

Intracellular localization analysis demonstrated a relatively high level of localization within lysosomes and little to no

https://doi.org/10.1021/acsanm.5c03169
ACS Appl. Nano Mater. 2025, 8, 16540−16552

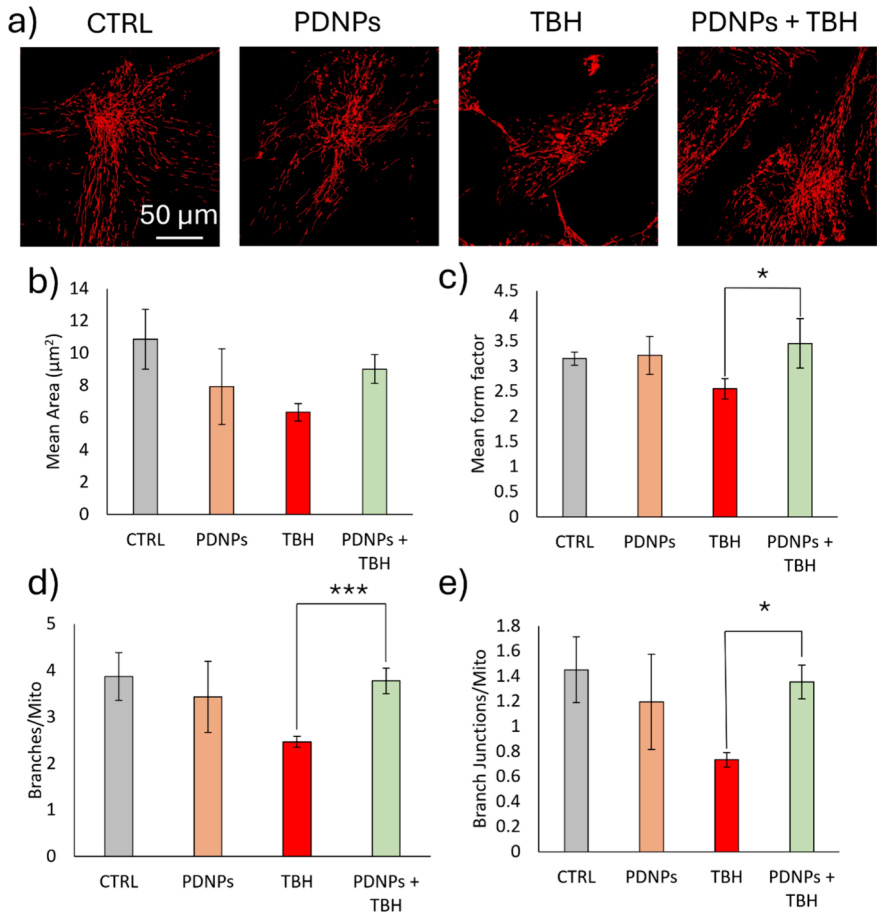

Figure 7. Analysis of mitochondrial morphology in MELAS-derived fibroblasts upon different experimental treatments: (a) representative confocal images and quantitative analysis of the (b) mitochondrial area, (c) mean form factor, (d) ratio between mitochondrial branches and mitochondria number, (e) ratio between branch junctions and mitochondria number (*$p < 0.05$, ***$p < 0.001$).

localization within mitochondria. The compartmentalization of polydopamine nanostructures within lysosomes is in line with other analyses present in the literature carried out on other cell types.[11,35,53] It is interesting to note that despite the little to no localization of PDNPs within mitochondria, a protective effect of the nanostructures from ROS-induced mitochondrial morphological aberrations has been observed. Several mechanisms could explain this phenomenon; for example, PDNPs could be acting on cytosolic ROS, which are known to diffuse out of mitochondria into the cytoplasm.[54] By scavenging these cytosolic ROS, PDNPs lower overall intracellular oxidative stress, indirectly protecting mitochondrial membranes, proteins, and DNA from damage. Additionally, the redox-active catechol and quinone groups of PDNPs could facilitate the sustained neutralization of ROS without requiring direct mitochondrial localization.[55] Similar indirect antioxidant effects have been described for other nanomaterials that remain in endolysosomal compartments, yet still preserve mitochondrial function by maintaining cellular redox balance.[9,56] As expected, a different susceptibility of patients' cells to ROS-induced damage was observed with respect to cells derived from healthy subjects: the treatment with TBH caused the accumulation of a higher amount of ROS in patient-derived cells, and an overall higher level of necrotic cells. This is in line with the higher levels of oxidative stress and the lower amount of endogenous antioxidant defense mechanisms observed in clinical studies carried out on both MELAS and PEO patients.[57,58] This notwithstanding, PDNPs were able to reduce the basal levels of ROS in both MELAS- and PEO-derived cells, and to partially counteract the increment of ROS induced by the treatment with TBH. The antioxidant activity of PDNPs observed in this work outperformed the efficiency of other antioxidant compounds tested on cells derived from patients affected by mitochondrial disorders, such as idebenone and resveratrol.[8,59]

The ability of PDNPs to prevent ROS-induced mitochondrial aberrations was investigated: ROS-induced damages can indeed interfere with the physiological organization and morphology of mitochondria, leading to impaired mitochondrial activities, further ROS production, and eventual cellular death. Moreover, as previously discussed, mitochondrial disorders, including MELAS and PEO diseases, are associated with an altered organization and morphology of the mitochondrial network caused by DNA and mtDNA mutations. One of the most common mitochondrial morphological aberrations induced by ROS is the change in shape from tubular to round/globular, with the consequent loss of mitochondrial branches and/or junctions.[60] Our results indicate that the treatment with TBH induces a change in shape from tubular to globular, which is associated with ROS-induced damage. This is in line with other regarding the effects of TBH on mitochondrial morphology.[17,35] The treatment with PDNPs was able to partially prevent these changes, and once again the particles showed different extents of efficiency on the three considered cell lines, most probably because of the already cited lower levels of endogenous

https://doi.org/10.1021/acsanm.5c03169
ACS Appl. Nano Mater. 2025, 8, 16540−16552

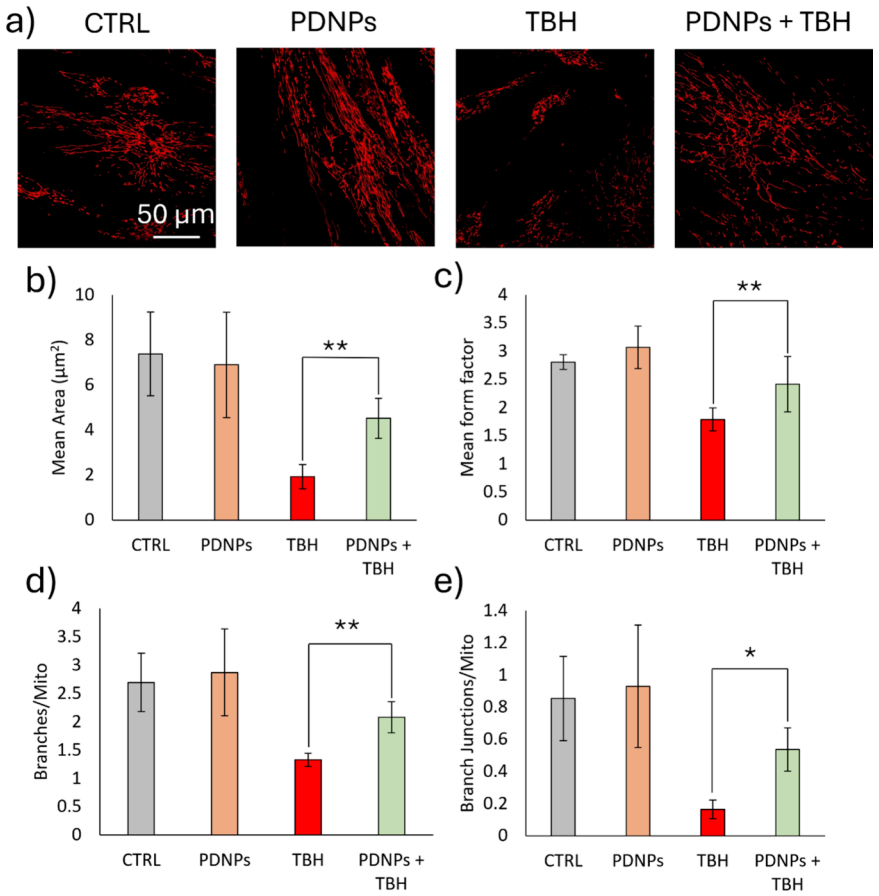

Figure 8. Analysis of mitochondrial morphology in PEO-derived fibroblasts upon different experimental treatments: (a) representative confocal images and quantitative analysis of the (b) mitochondrial area, (c) mean form factor, (d) ratio between mitochondrial branches and mitochondria number, (e) ratio between branch junctions and mitochondria number (*$p < 0.05$, **$p < 0.01$).

antioxidant defenses associated with the two disorders[57,58]: in this respect, PDNPs could represent a promising tool to prevent the exacerbation of the mitochondrial dysfunctions present in MELAS and PEO patients.

The antioxidant properties of PDNPs were eventually in vivo tested on zebrafish embryos. Zebrafish is commonly exploited as an animal model to assess the antioxidant efficiency of various compounds, due to the high susceptibility of these animals to pro-oxidative damage. Some examples include treatments with naringenin, apigenin, rutin, oleuropein, chlorogenic acid, curcumin, lycopene B, β-carotene, and astaxanthin.[61] Our results showed that PDNPs can decrease the endogenous ROS levels in zebrafish embryos, and drastically reduce the oxidative stress induced by the treatment of the animals with TBH. PDNPs indeed showed a higher antioxidant efficiency on zebrafish, when compared with other compounds such as morin and RW20 peptide, thus confirming their outstanding protective effects.[62,63]

The comparison between PDNPs and conventional antioxidants such as N-acetylcysteine (NAC), vitamin E, and coenzyme Q10 highlights several important distinctions. Conventional antioxidants primarily act as small-molecule nucleophilic scavengers or chain-breaking antioxidants: NAC functions not only by replenishing intracellular glutathione pools and reducing disulfide bonds, but also through the generation of hydrogen−sulfur species that contribute to redox regulation and cytoprotection[64]; vitamin E mainly acts as a lipid-soluble peroxyl radical scavenger interrupting lipid peroxidation chain reactions in membranes[65]; coenzyme Q10 serves as an electron carrier in the mitochondrial respiratory chain while also scavenging free radicals and stabilizing mitochondrial function.[65] Conversely, PDNPs exert their antioxidant effects via multiple mechanisms, including persistent radical scavenging by catechol and quinone groups,[55] chelation of transition metals, and regenerative redox cycling,[66] which enable prolonged neutralization of ROS even under sustained oxidative stress. Furthermore, small-molecule antioxidants often show rapid systemic clearance and limited tissue retention, which can reduce their therapeutic window. Due to their nanostructured form and versatile surface chemistry, PDNPs exhibit enhanced bioadhesiveness, slower degradation kinetics, and the potential to accumulate more selectively in target tissues, including the nervous system.[11] Notably, their fully organic and biodegradable composition reduces concerns about long-term toxicity and facilitates excretion from the body, supporting their translational potential as safer, multifunctional antioxidant platforms.[11]

5. CONCLUSIONS

Collected results demonstrate the potential of PDNPS as a nonpharmaceutical antioxidant treatment for both MELAS and PEO diseases. PDNPs were indeed able to reduce the oxidative stress associated with both disorders and to protect the cells from pro-oxidant-induced cellular death. Moreover, PDNPs were also able to prevent mitochondrial morphological aberrations induced by the treatment with a pro-oxidant agent. PDNPs were eventually found to be able to reduce the ROS

https://doi.org/10.1021/acsanm.5c03169
ACS Appl. Nano Mater. 2025, 8, 16540−16552

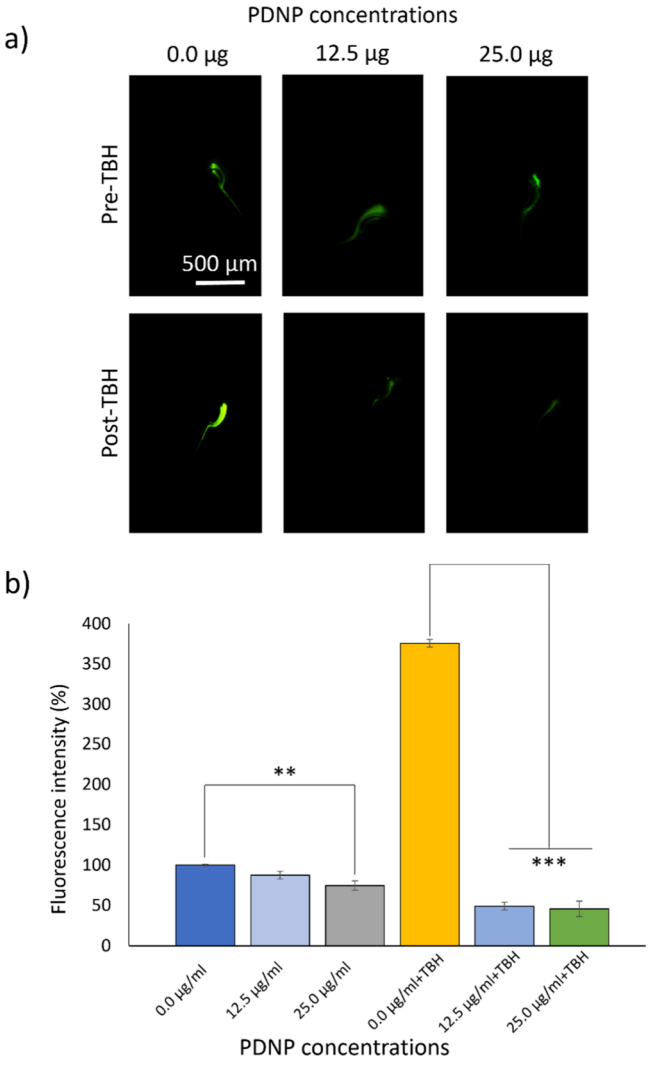

Figure 9. Analysis of PDNP antioxidant activity on zebrafish embryos upon different experimental treatments. (a) Representative fluorescence images after H2DCFDA staining and (b) quantitative analysis of fluorescence (and thus ROS) levels before and after TBH treatment (**$p < 0.01$, ***$p < 0.001$).

levels in zebrafish embryos and to protect the animals from the oxidative stress induced by a pro-oxidant TBH treatment. Future development of this work could involve the following points.

The testing of PDNPs on in vivo models of mitochondrial disorders, for example, by exploiting transgenic zebrafish embryos. While the present study demonstrates the antioxidant and cytoprotective effects of PDNPs in vitro and in a general oxidative stress zebrafish model, we recognize that further validation in disease-specific in vivo systems would strengthen the translational relevance of these findings. Future studies employing established MELAS and PEO animal models will be essential to confirm the therapeutic potential of PDNPs in the context of mitochondrial DNA mutations and to assess their impact on mitochondrial bioenergetics and tissue-level pathology. These investigations are planned as a continuation of this work: for example, CRISPR/Cas9-generated zebrafish knockout models that replicate the key hallmarks of both diseases could represent a crucial next step in evaluating the therapeutic potential of PDNPs.[67]

The testing of various surface functionalizations of PDNPs to optimize their bioavailability and BBB-crossing efficiency. In previous work from our group, we demonstrated that PDNPs with diameters as large as 200 nm were capable of traversing in vitro models of the BBB without the need for any additional functionalization.[17,35] We hypothesize that this capacity is mediated by adsorptive-mediated transcytosis, a mechanism well-established for nanostructures in the 50−200 nm size range.[68] In addition, it has been proposed that the catechol and amine groups of polydopamine can promote strong interactions with cellular membranes, thereby enhancing internalization via endocytosis and transcytosis.[55] Furthermore, PDNPs have been shown to readily adsorb serum proteins, forming a protein corona that may further facilitate recognition and transport across the BBB.[46] Despite the intrinsic potential of unmodified PDNPs to cross the BBB, studies may be addressed to explore surface decoration with targeting ligands such as apolipoprotein E (ApoE) or angiopep-2 to enhance CNS delivery and therapeutic efficacy further.

Final aspects regard the development and testing of strategies for the mitochondrial targeting of PDNPs, in order to improve their efficiency against mitochondrial pathologies while minimizing potential off-target adverse effects, and the development of a large-scale synthesis method to increase the production of PDNPs, granting their exploitation in clinical trials.

■ ASSOCIATED CONTENT

Data Availability Statement

Proteomics data are available via ProteomeXchange with identifier PXD063824. [Reviewer account details: Username: reviewer_pxd063824@ebi.ac.uk; Password: ciFf7yZJ4rhE]. All other data are available from the authors upon reasonable request.

Supporting Information

The Supporting Information is available free of charge at https://pubs.acs.org/doi/10.1021/acsanm.5c03169.

Proteomic analysis; representative confocal images and quantitative analysis of live/dead assay; PicoGreen analysis on cells treated with various concentrations of PDNPs; representative histograms of flow cytometry analysis showing the internalization of DiO-PDNPs; representative confocal images showing the intracellular localization of PDNPs; representative histograms of flow cytometry measurements regarding ROS analysis; representative scatter plot flow cytometry measurements regarding apoptosis/necrosis analysis; a Table reporting complete statistical analysis on ROS evaluation (PDF)

■ AUTHOR INFORMATION

Corresponding Authors

Matteo Battaglini − *Smart Bio-Interfaces, Istituto Italiano di Tecnologia, 56025 Pontedera, Italy*; Email: matteo.battaglini@iit.it

Gianni Ciofani − *Smart Bio-Interfaces, Istituto Italiano di Tecnologia, 56025 Pontedera, Italy*; orcid.org/0000-0003-1192-3647; Email: gianni.ciofani@iit.it

Authors

Francesco Schiavone − *Smart Bio-Interfaces, Istituto Italiano di Tecnologia, 56025 Pontedera, Italy*

https://doi.org/10.1021/acsanm.5c03169
ACS Appl. Nano Mater. 2025, 8, 16540−16552

Alessio Carmignani − *Smart Bio-Interfaces, Istituto Italiano di Tecnologia, 56025 Pontedera, Italy;* orcid.org/0000-0002-6316-3478
Attilio Marino − *Smart Bio-Interfaces, Istituto Italiano di Tecnologia, 56025 Pontedera, Italy;* orcid.org/0000-0002-3290-494X
Valentina Naef − *Neurobiology and Molecular Medicine Unit, IRCCS Fondazione Stella Maris, 56128 Calambrone (Pisa), Italy*
Andrea Petretto − *Core Facilities-Clinical Proteomics and Metabolomics, IRCCS Istituto Giannina Gaslini, 16147 Genova, Italy;* orcid.org/0000-0001-7811-8517
Martina Bartolucci − *Core Facilities-Clinical Proteomics and Metabolomics, IRCCS Istituto Giannina Gaslini, 16147 Genova, Italy;* orcid.org/0000-0001-5289-4219
Fabiana Longo − *Mitochondrial Dysfunctions in Neurodegeneration Unit, Division of Neuroscience, IRCCS Ospedale San Raffaele, 20132 Milano, Italy; Università Vita-Salute San Raffaele, 20132 Milano, Italy*
Francesca Maltecca − *Mitochondrial Dysfunctions in Neurodegeneration Unit, Division of Neuroscience, IRCCS Ospedale San Raffaele, 20132 Milano, Italy; Università Vita-Salute San Raffaele, 20132 Milano, Italy*
Filippo Maria Santorelli − *Neurobiology and Molecular Medicine Unit, IRCCS Fondazione Stella Maris, 56128 Calambrone (Pisa), Italy*

Complete contact information is available at: https://pubs.acs.org/10.1021/acsanm.5c03169

Author Contributions

M.B.: conceptualization; investigation; methodology; validation; conceptualization; data curation; formal analysis; writing-original draft; F.S.: methodology; data curation; A.C.: methodology; data curation; formal analysis; A.M.: methodology; data curation; formal analysis; V.N.: methodology; validation; data curation; formal analysis; A.P.: resources; methodology; validation; data curation; formal analysis; M.B.: validation; data curation; formal analysis; F.L.: methodology; data curation; formal analysis; F.M.: conceptualization; resources; supervision; F.M.S.: conceptualization; resources; supervision; G.C.: conceptualization; resources; supervision; project administration; writing-review and editing.

Notes

The authors declare no competing financial interest.

■ ACKNOWLEDGMENTS

Authors would like to thank Dr. F. Catalano and Dr. R. Brescia (Italian Institute of Technology, Italy) for their kind assistance in TEM imaging, and prof. S. Previtali (IRCCS Ospedale San Raffaele, Milano) for providing skin biopsies of patients.

■ REFERENCES

(1) Gorman, G. S.; Chinnery, P. F.; DiMauro, S.; Hirano, M.; Koga, Y.; McFarland, R.; Suomalainen, A.; Thorburn, D. R.; Zeviani, M.; Turnbull, D. M. Mitochondrial Diseases. *Nat. Rev. Dis Primers* **2016**, *2* (1), 16080.
(2) Rose, S.; Niyazov, D. M.; Rossignol, D. A.; Goldenthal, M.; Kahler, S. G.; Frye, R. E. Clinical and Molecular Characteristics of Mitochondrial Dysfunction in Autism Spectrum Disorder. *Mol. Diagn Ther* **2018**, *22* (5), 571−593.
(3) Li, Y.; Berliocchi, L.; Li, Z.; Rasmussen, L. J. Interactions between Mitochondrial Dysfunction and Other Hallmarks of Aging: Paving a Path toward Interventions That Promote Healthy Old Age. *Aging Cell* **2024**, *23* (1), No. e13942.
(4) Tao, W.; Zhang, H.; Jiang, X.; Chen, N. Resveratrol Combats Chronic Diseases through Enhancing Mitochondrial Quality. *Food Science and Human Wellness* **2024**, *13* (2), 597−610.
(5) Jaber, S. M.; Ge, S. X.; Milstein, J. L.; VanRyzin, J. W.; Waddell, J.; Polster, B. M. Idebenone Has Distinct Effects on Mitochondrial Respiration in Cortical Astrocytes Compared to Cortical Neurons Due to Differential NQO1 Activity. *J. Neurosci.* **2020**, *40* (23), 4609−4619.
(6) Wright, D. J.; Renoir, T.; Smith, Z. M.; Frazier, A. E.; Francis, P. S.; Thorburn, D. R.; McGee, S. L.; Hannan, A. J.; Gray, L. J. N-Acetylcysteine Improves Mitochondrial Function and Ameliorates Behavioral Deficits in the R6/1 Mouse Model of Huntington's Disease. *Transl Psychiatry* **2015**, *5* (1), No. e492.
(7) Martinelli, C.; Pucci, C.; Battaglini, M.; Marino, A.; Ciofani, G. Antioxidants and Nanotechnology: Promises and Limits of Potentially Disruptive Approaches in the Treatment of Central Nervous System Diseases. *Adv. Healthc Mater.* **2020**, *9* (3), No. 1901589.
(8) Martinelli, C.; Battaglini, M.; Pucci, C.; Gioi, S.; Caracci, C.; Macaluso, G.; Doccini, S.; Santorelli, F. M.; Ciofani, G. Development of Nanostructured Lipid Carriers for the Delivery of Idebenone in Autosomal Recessive Spastic Ataxia of Charlevoix-Saguenay. *ACS Omega* **2020**, *5* (21), 12451−12466.
(9) Pezzini, I.; Marino, A.; Del Turco, S.; Nesti, C.; Doccini, S.; Cappello, V.; Gemmi, M.; Parlanti, P.; Santorelli, F. M.; Mattoli, V.; Ciofani, G. Cerium Oxide Nanoparticles: The Regenerative Redox Machine in Bioenergetic Imbalance. *Nanomedicine* **2017**, *12* (4), 403−416.
(10) Yang, J.; Du, L.; Guo, J.; Zhang, L.; Wang, S.; Wang, X. Injectable Carboxymethyl Chitosan/Konjac Glucomannan/Catechin Hydrogel with Free Radical-Scavenging, Antimicrobial, and pro-Healing Abilities for Infected Wound Repair. *Int. J. Biol. Macromol.* **2025**, *308*, No. 142572.
(11) Battaglini, M.; Emanet, M.; Carmignani, A.; Ciofani, G. Polydopamine-Based Nanostructures: A New Generation of Versatile, Multi-Tasking, and Smart Theranostic Tools. *Nano Today* **2024**, *55*, No. 102151.
(12) Vong, L. B.; Sato, Y.; Chonpathompikunlert, P.; Tanasawet, S.; Hutamekalin, P.; Nagasaki, Y. Self-Assembled Polydopamine Nanoparticles Improve Treatment in Parkinson's Disease Model Mice and Suppress Dopamine-Induced Dyskinesia. *Acta Biomater* **2020**, *109*, 220−228.
(13) Chen, X.; Gao, W.; Sun, Y.; Dong, X. Multiple Effects of Polydopamine Nanoparticles on Cu2+-Mediated Alzheimer's β-Amyloid Aggregation. *Chin J. Chem. Eng.* **2023**, *54*, 144−152.
(14) Jian, C.; Hong, Y.; Liu, H.; Yang, Q.; Zhao, S. ROS-Responsive Quercetin-Based Polydopamine Nanoparticles for Targeting Ischemic Stroke by Attenuating Oxidative Stress and Neuroinflammation. *Int. J. Pharm.* **2025**, *669*, No. 125087.
(15) Carmignani, A.; Battaglini, M.; Bartolucci, M.; Petretto, A.; Prato, M.; Ciofani, G. Polydopamine Nanoparticles as a Non-Pharmaceutical Tool in the Treatment of Fatty Liver Disease. *Mater. Des* **2024**, *239*, No. 112825.
(16) Sun, H.; Wang, Y.; He, T.; He, D.; Hu, Y.; Fu, Z.; Wang, Y.; Sun, D.; Wang, J.; Liu, Y.; Shu, L.; He, L.; Deng, Z.; Yang, X. Hollow Polydopamine Nanoparticles Loading with Peptide RL-QN15: A New pro-Regenerative Therapeutic Agent for Skin Wounds. *J. Nanobiotechnology* **2021**, *19* (1), 304.
(17) Battaglini, M.; Carmignani, A.; Martinelli, C.; Colica, J.; Marino, A.; Doccini, S.; Mollo, V.; Santoro, F.; Bartolucci, M.; Petretto, A.; Santorelli, F. M.; Ciofani, G. In Vitro Study of Polydopamine Nanoparticles as Protective Antioxidant Agents in Fibroblasts Derived from ARSACS Patients. *Biomater Sci.* **2022**, *10* (14), 3770−3792.
(18) El-Hattab, A. W.; Adesina, A. M.; Jones, J.; Scaglia, F. MELAS Syndrome: Clinical Manifestations, Pathogenesis, and Treatment Options. *Mol. Genet. Metab.* **2015**, *116* (1−2), 4−12.
(19) Hirano, M.; Pitceathly, R. D. S. Progressive External Ophthalmoplegia. *Handb. Clin. Neurol.* **2023**, *194*, 9−21.

(20) Heighton, J. N.; Brady, L. I.; Sadikovic, B.; Bulman, D. E.; Tarnopolsky, M. A. Genotypes of Chronic Progressive External Ophthalmoplegia in a Large Adult-Onset Cohort. *Mitochondrion* **2019**, *49*, 227−231.
(21) Hayashi, G.; Cortopassi, G. Oxidative Stress in Inherited Mitochondrial Diseases. *Free Radic Biol. Med.* **2015**, *88*, 10−17.
(22) Lewis, W.; Day, B. J.; Kohler, J. J.; Hosseini, S. H.; Chan, S. S. L.; Green, E. C.; Haase, C. P.; Keebaugh, E. S.; Long, R.; Ludaway, T.; Russ, R.; Steltzer, J.; Tioleco, N.; Santoianni, R.; Copeland, W. C. Decreased MtDNA, Oxidative Stress, Cardiomyopathy, and Death from Transgenic Cardiac Targeted Human Mutant Polymerase γ. *Laboratory Investigation* **2007**, *87* (4), 326−335.
(23) Bartsakoulia, M.; Müller, J. S.; Gomez-Duran, A.; Yu-Wai-Man, P.; Boczonadi, V.; Horvath, R. Cysteine Supplementation May Be Beneficial in a Subgroup of Mitochondrial Translation Deficiencies. *J. Neuromuscul. Dis.* **2016**, *3* (3), 363−379.
(24) De Paepe, B.; Van Coster, R. A Critical Assessment of the Therapeutic Potential of Resveratrol Supplements for Treating Mitochondrial Disorders. *Nutrients* **2017**, *9* (9), 1017.
(25) Ikejiri, Y.; Mori, E.; Ishii, K.; Nishimoto, K.; Yasuda, M.; Sasaki, M. Idebenone Improves Cerebral Mitochondrial Oxidative Metabolism in a Patient with MELAS. *Neurology* **1996**, *47* (2), 583−585.
(26) Barros, C. D. S.; Coutinho, A.; Tengan, C. H. Arginine Supplementation in MELAS Syndrome: What Do We Know about the Mechanisms? *Int. J. Mol. Sci.* **2024**, *25* (7), 3629.
(27) Ali, A.; Esmaeil, A.; Behbehani, R. Mitochondrial Chronic Progressive External Ophthalmoplegia. *Brain Sci.* **2024**, *14* (2), 135.
(28) Acter, S.; Vidallon, M. L. P.; Crawford, S.; Tabor, R. F.; Teo, B. M. Bowl-Shaped Mesoporous Polydopamine Nanoparticles for Size-Dependent Endocytosis into HeLa Cells. *ACS Appl. Nano Mater.* **2021**, *4* (9), 9536−9546.
(29) Ding, L.; Zhu, X.; Wang, Y.; Shi, B.; Ling, X.; Chen, H.; Nan, W.; Barrett, A.; Guo, Z.; Tao, W.; Wu, J.; Shi, X. Intracellular Fate of Nanoparticles with Polydopamine Surface Engineering and a Novel Strategy for Exocytosis-Inhibiting, Lysosome Impairment-Based Cancer Therapy. *Nano Lett.* **2017**, *17* (11), 6790−6801.
(30) Sanchez, N.; Chapdelaine, P.; Rousseau, J.; Raymond, F.; Corbeil, J.; Tremblay, J. P. Characterization of Frataxin Gene Network in Friedreich's Ataxia Fibroblasts Using the RNA-Seq Technique. *Mitochondrion* **2016**, *30*, 59−66.
(31) Tokuyama, T.; Hirai, A.; Shiiba, I.; Ito, N.; Matsuno, K.; Takeda, K.; Saito, K.; Mii, K.; Matsushita, N.; Fukuda, T.; Inatome, R.; Yanagi, S. Mitochondrial Dynamics Regulation in Skin Fibroblasts from Mitochondrial Disease Patients. *Biomolecules* **2020**, *10* (3), 450.
(32) Olesen, M. A.; Villavicencio-Tejo, F.; Quintanilla, R. A. The Use of Fibroblasts as a Valuable Strategy for Studying Mitochondrial Impairment in Neurological Disorders. *Transl Neurodegener* **2022**, *11* (1), 36.
(33) Correia, S. P.; Moedas, M. F.; Taylor, L. S.; Naess, K.; Lim, A. Z.; McFarland, R.; Kazior, Z.; Rumyantseva, A.; Wibom, R.; Engvall, M.; Bruhn, H.; Lesko, N.; Végvári, Á.; Käll, L.; Trost, M.; Alston, C. L.; Freyer, C.; Taylor, R. W.; Wedell, A.; Wredenberg, A. Quantitative Proteomics of Patient Fibroblasts Reveal Biomarkers and Diagnostic Signatures of Mitochondrial Disease. *JCI Insight* **2024**, *9* (20), No. e178645.
(34) Bakare, A. B.; Daniel, J.; Stabach, J.; Rojas, A.; Bell, A.; Henry, B.; Iyer, S. Quantifying Mitochondrial Dynamics in Patient Fibroblasts with Multiple Developmental Defects and Mitochondrial Disorders. *Int. J. Mol. Sci.* **2021**, *22* (12), 6263.
(35) Battaglini, M.; Marino, A.; Carmignani, A.; Tapeinos, C.; Cauda, V.; Ancona, A.; Garino, N.; Vighetto, V.; La Rosa, G.; Sinibaldi, E.; Ciofani, G. Polydopamine Nanoparticles as an Organic and Biodegradable Multitasking Tool for Neuroprotection and Remote Neuronal Stimulation. *ACS Appl. Mater. Interfaces* **2020**, *12* (33), 35782−35798.
(36) Bekker-Jensen, D. B.; Martínez-Val, A.; Steigerwald, S.; Rüther, P.; Fort, K. L.; Arrey, T. N.; Harder, A.; Makarov, A.; Olsen, J. V. A Compact Quadrupole-Orbitrap Mass Spectrometer with FAIMS Interface Improves Proteome Coverage in Short LC Gradients. *Molecular & Cellular Proteomics* **2020**, *19* (4), 716−729.
(37) Kimmel, C. B.; Ballard, W. W.; Kimmel, S. R.; Ullmann, B.; Schilling, T. F. Stages of Embryonic Development of the Zebrafish. *Dev. Dyn.* **1995**, *203* (3), 253−310.
(38) Naef, V.; Lieto, M.; Satolli, S.; De Micco, R.; Troisi, M.; Pasquariello, R.; Doccini, S.; Privitera, F.; Filla, A.; Tessitore, A.; Santorelli, F. M. SCAR32: Functional Characterization and Expansion of the Clinical-Genetic Spectrum. *Ann. Clin Transl Neurol* **2024**, *11* (7), 1879−1886.
(39) Naef, V.; Marchese, M.; Ogi, A.; Fichi, G.; Galatolo, D.; Licitra, R.; Doccini, S.; Verri, T.; Argenton, F.; Morani, F.; Santorelli, F. M. Efficient Neuroprotective Rescue of Sacsin-Related Disease Phenotypes in Zebrafish. *Int. J. Mol. Sci.* **2021**, *22* (16), 8401.
(40) Lackmann, C.; Santos, M. M.; Rainieri, S.; Barranco, A.; Hollert, H.; Spirhanzlova, P.; Velki, M.; Seiler, T.-B. Novel Procedures for Whole Organism Detection and Quantification of Fluorescence as a Measurement for Oxidative Stress in Zebrafish (Danio Rerio) Larvae. *Chemosphere* **2018**, *197*, 200−209.
(41) Bruderer, R.; Bernhardt, O. M.; Gandhi, T.; Miladinović, S. M.; Cheng, L.-Y.; Messner, S.; Ehrenberger, T.; Zanotelli, V.; Butscheid, Y.; Escher, C.; Vitek, O.; Rinner, O.; Reiter, L. Extending the Limits of Quantitative Proteome Profiling with Data-Independent Acquisition and Application to Acetaminophen-Treated Three-Dimensional Liver Microtissues. *Molecular & Cellular Proteomics* **2015**, *14* (5), 1400−1410.
(42) Tyanova, S.; Temu, T.; Sinitcyn, P.; Carlson, A.; Hein, M. Y.; Geiger, T.; Mann, M.; Cox, J. The Perseus Computational Platform for Comprehensive Analysis of (Prote)Omics Data. *Nat. Methods* **2016**, *13* (9), 731−740.
(43) Greene, C. S.; Krishnan, A.; Wong, A. K.; Ricciotti, E.; Zelaya, R. A.; Himmelstein, D. S.; Zhang, R.; Hartmann, B. M.; Zaslavsky, E.; Sealfon, S. C.; Chasman, D. I.; FitzGerald, G. A.; Dolinski, K.; Grosser, T.; Troyanskaya, O. G. Understanding Multicellular Function and Disease with Human Tissue-Specific Networks. *Nat. Genet.* **2015**, *47* (6), 569−576.
(44) Carmignani, A.; Battaglini, M.; Sinibaldi, E.; Marino, A.; Vighetto, V.; Cauda, V.; Ciofani, G. In Vitro and Ex Vivo Investigation of the Effects of Polydopamine Nanoparticle Size on Their Antioxidant and Photothermal Properties: Implications for Biomedical Applications. *ACS Appl. Nano Mater.* **2022**, *5* (1), 1702−1713.
(45) Manzanares, D.; Ceña, V. Endocytosis: The Nanoparticle and Submicron Nanocompounds Gateway into the Cell. *Pharmaceutics* **2020**, *12* (4), 371.
(46) Battaglini, M.; Carmignani, A.; Ciobanu, D. Z.; Marino, A.; Catalano, F.; Armirotti, A.; Ciofani, G. Detailed Profiling of Protein Corona Formed by Polydopamine Nanoparticles in Human Plasma. *ACS Appl. Mater. Interfaces* **2025**, *17* (7), 10485−10498.
(47) Chen, N.; Yao, S.; Li, M.; Wang, Q.; Sun, X.; Feng, X.; Chen, Y. Nonporous versus Mesoporous Bioinspired Polydopamine Nanoparticles for Skin Drug Delivery. *Biomacromolecules* **2023**, *24* (4), 1648−1661.
(48) Koga, Y.; Povalko, N.; Nishioka, J.; Katayama, K.; Yatsuga, S.; Matsuishi, T. Molecular Pathology of MELAS and L-Arginine Effects. *Biochimica et Biophysica Acta (BBA) - General Subjects* **2012**, *1820* (5), 608−614.
(49) Li, H.; Uittenbogaard, M.; Navarro, R.; Ahmed, M.; Gropman, A.; Chiaramello, A.; Hao, L. Integrated Proteomic and Metabolomic Analyses of the Mitochondrial Neurodegenerative Disease MELAS. *Mol. Omics* **2022**, *18* (3), 196−205.
(50) Santacatterina, F.; Torresano, L.; Núñez-Salgado, A.; Esparza-Molto, P. B.; Olive, M.; Gallardo, E.; García-Arumi, E.; Blazquez, A.; González-Quintana, A.; Martín, M. A.; Cuezva, J. M. Different Mitochondrial Genetic Defects Exhibit the Same Protein Signature of Metabolism in Skeletal Muscle of PEO and MELAS Patients: A Role for Oxidative Stress. *Free Radic Biol. Med.* **2018**, *126*, 235−248.
(51) Geffroy, G.; Benyahia, R.; Frey, S.; Desquiret-Dumas, V.; Gueguen, N.; Bris, C.; Belal, S.; Inisan, A.; Renaud, A.; Chevrollier, A.; Henrion, D.; Bonneau, D.; Letournel, F.; Lenaers, G.; Reynier, P.;

https://doi.org/10.1021/acsanm.5c03169
ACS Appl. Nano Mater. 2025, 8, 16540−16552

Procaccio, V. The Accumulation of Assembly Intermediates of the Mitochondrial Complex I Matrix Arm Is Reduced by Limiting Glucose Uptake in a Neuronal-like Model of MELAS Syndrome. *Biochim. Biophys. Acta (BBA) - Mol. Basis Dis.* **2018**, *1864* (5), 1596−1608.
(52) DiFrancesco, J. C.; Cooper, J. M.; Lam, A.; Hart, P. E.; Tremolizzo, L.; Ferrarese, C.; Schapira, A. H. MELAS Mitochondrial DNA Mutation A3243G Reduces Glutamate Transport in Cybrids Cell Lines. *Exp. Neurol.* **2008**, *212* (1), 152−156.
(53) Carmignani, A.; Battaglini, M.; Marino, A.; Pignatelli, F.; Ciofani, G. Drug-Loaded Polydopamine Nanoparticles for Chemo/Photothermal Therapy against Colorectal Cancer Cells. *ACS Appl. Bio Mater.* **2024**, *7* (4), 2205−2217.
(54) Murphy, M. P. How Mitochondria Produce Reactive Oxygen Species. *Biochem Jl* **2009**, *417* (1), 1−13.
(55) Liu, Y.; Ai, K.; Lu, L. Polydopamine and Its Derivative Materials: Synthesis and Promising Applications in Energy, Environmental, and Biomedical Fields. *Chem. Rev.* **2014**, *114* (9), 5057−5115.
(56) Liu, Y.; Ai, K.; Ji, X.; Askhatova, D.; Du, R.; Lu, L.; Shi, J. Comprehensive Insights into the Multi-Antioxidative Mechanisms of Melanin Nanoparticles and Their Application To Protect Brain from Injury in Ischemic Stroke. *J. Am. Chem. Soc.* **2017**, *139* (2), 856−862.
(57) Katayama, Y.; Maeda, K.; Iizuka, T.; Hayashi, M.; Hashizume, Y.; Sanada, M.; Kawai, H.; Kashiwagi, A. Accumulation of Oxidative Stress around the Stroke-like Lesions of MELAS Patients. *Mitochondrion* **2009**, *9* (5), 306−313.
(58) Piccolo, G.; Banfi, P.; Azan, G.; Rizzuto, R.; Bisson, R.; Sandoná, D.; Bellomo, G. Biological Markers of Oxidative Stress in Mitochondrial Myopathies with Progressive External Ophthalmoplegia. *J. Neurol Sci.* **1991**, *105* (1), 57−60.
(59) Şen, Ö.; Emanet, M.; Marino, A.; Belenli Gümüş, M.; Bartolucci, M.; Doccini, S.; Catalano, F.; Genchi, G. G.; Santorelli, F. M.; Petretto, A.; Ciofani, G. Evaluation of the Therapeutic Potential of Resveratrol-Loaded Nanostructured Lipid Carriers on Autosomal Recessive Spastic Ataxia of Charlevoix-Saguenay Patient-Derived Fibroblasts. *Mater. Des* **2021**, *209*, No. 110012.
(60) Ahmad, T.; Aggarwal, K.; Pattnaik, B.; Mukherjee, S.; Sethi, T.; Tiwari, B. K.; Kumar, M.; Micheal, A.; Mabalirajan, U.; Ghosh, B.; Sinha Roy, S.; Agrawal, A. Computational Classification of Mitochondrial Shapes Reflects Stress and Redox State. *Cell Death Dis* **2013**, *4* (1), No. e461.
(61) Arteaga, C.; Boix, N.; Teixido, E.; Marizande, F.; Cadena, S.; Bustillos, A. The Zebrafish Embryo as a Model to Test Protective Effects of Food Antioxidant Compounds. *Molecules* **2021**, *26* (19), 5786.
(62) Prabha, N.; Guru, A.; Harikrishnan, R.; Gatasheh, M. K.; Hatamleh, A. A.; Juliet, A.; Arockiaraj, J. Neuroprotective and Antioxidant Capability of RW20 Peptide from Histone Acetyltransferases Caused by Oxidative Stress-Induced Neurotoxicity in in Vivo Zebrafish Larval Model. *J. King Saud Univ Sci.* **2022**, *34* (3), No. 101861.
(63) Issac, P. K.; Guru, A.; Velayutham, M.; Pachaiappan, R.; Arasu, M. V.; Al-Dhabi, N. A.; Choi, K. C.; Harikrishnan, R.; Arockiaraj, J. Oxidative Stress Induced Antioxidant and Neurotoxicity Demonstrated in Vivo Zebrafish Embryo or Larval Model and Their Normalization Due to Morin Showing Therapeutic Implications. *Life Sci.* **2021**, *283*, No. 119864.
(64) Pedre, B.; Barayeu, U.; Ezeriņa, D.; Dick, T. P. The Mechanism of Action of N-Acetylcysteine (NAC): The Emerging Role of H2S and Sulfane Sulfur Species. *Pharmacol Ther* **2021**, *228*, No. 107916.
(65) Niki, E. Role of Vitamin E as a Lipid-Soluble Peroxyl Radical Scavenger: In Vitro and in Vivo Evidence. *Free Radic. Biol. Med.* **2014**, *66*, 3−12.
(66) Ju, K.-Y.; Lee, Y.; Lee, S.; Park, S. B.; Lee, J.-K. Bioinspired Polymerization of Dopamine to Generate Melanin-Like Nanoparticles Having an Excellent Free-Radical-Scavenging Property. *Biomacromol* **2011**, *12* (3), 625−632.
(67) Brañas Casas, R.; Zuppardo, A.; Risato, G.; Dinarello, A.; Celeghin, R.; Fontana, C.; Grelloni, E.; Gilea, A. I.; Viscomi, C.; Rasola, A.; Dalla Valle, L.; Lodi, T.; Baruffini, E.; Facchinello, N.; Argenton, F.; Tiso, N. Zebrafish Polg2 Knock-out Recapitulates Human POLG-Disorders; Implications for Drug Treatment. *Cell Death Dis* **2024**, *15* (4), 281.
(68) Saraiva, C.; Praça, C.; Ferreira, R.; Santos, T.; Ferreira, L.; Bernardino, L. Nanoparticle-Mediated Brain Drug Delivery: Overcoming Blood−Brain Barrier to Treat Neurodegenerative Diseases. *J. Controlled Release* **2016**, *235*, 34−47.

https://doi.org/10.1021/acsanm.5c03169
ACS Appl. Nano Mater. 2025, 8, 16540−16552